Journal of Materials Chemistry A

Accepted Manuscript

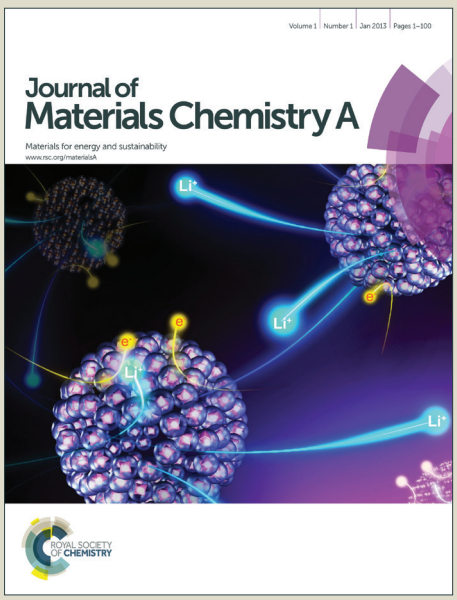

ROYAL SOCIETY OF CHEMISTRY

www.rsc.org/materialsA

Improving the energy density of $Na_3V_2(PO_4)_3$ – based positive electrodes through V / Al substitution

F. Lalère [1,2], V. Seznec [1,2], M. Courty [1,2], R. David [1,2], J. N. Chotard [1,2], C. Masquelier [1,2,#]

[1] *Laboratoire de Réactivité et de Chimie des Solides, CNRS-UMR#7314, Université de Picardie Jules Verne, F-80039 Amiens Cedex 1, France*

[2] *RS2E, Réseau Français sur le Stockage Electrochimique de l'Energie, FR CNRS 3459, France.*

Abstract

The crystal chemistry and the electrochemical properties upon Na^+ extraction/insertion of NASICON-type $Na_3Al_yV_{2-y}(PO_4)_3$ compositions (y = 0.1, 0.25 and 0.5) were investigated. It was found that this family of V/Al substituted NASICON materials undergoes multiple reversible phase transitions between -50°C and 250°C upon heating, from monoclinic to rhombohedral symmetry, related to progressive disordering of the Na^+ ions within the framework. The Na^+ insertion/extraction mechanisms were monitored by *operando* X-ray diffraction. It is shown for the first time that substitution of aluminum for vanadium in $Na_3Al_{0.5}V_{1.5}(PO_4)_3$ increases significantly the theoretical energy density of these promising positive electrodes (425 Wh/kg) due to a lighter molecular weight and to the possibility of reversible operation on the V^{4+}/V^{5+} redox couple at 3.95 V vs. Na^+/Na.

Introduction

NASICON-type vanadium phosphate $Na_3V^{III}_2(PO_4)_3$ (NVP) is an attractive cathode material for sodium-ion batteries, presently investigated in particular for its high power rate capabilities [1-7]. The reversible extraction of sodium occurs as a two-phase reaction at 3.37 V vs. Na^+/Na (V^{3+} oxidized to V^{4+}) for a theoretical gravimetric capacity of 117.6 mA.h/g yielding an energy density of 396 W.h/kg. To our knowledge, the first electrochemical investigation of this material was reported in 2002 [8] but only very recently Saravanan *et al.* [1] demonstrated excellent cyclability of NVP even at very high current rate thanks to the presence of a thin layer of carbon coating that compensates for the low electrical conductivity. Since then, several high-profile studies were conducted in order to obtain optimized performances [1-7].

Gopalakrishnan [9] was the first to report on the chemical oxidation of NASICON $Na_3V^{III}_2(PO_4)_3$ (Na^+ extraction) to yield a new Na-free mixed-valence $V^{V}V^{IV}(PO_4)_3$ composition, suggesting the theoretical extraction of 3 Na^+ per 2 vanadium (i.e. 1.5 e^- exchanged per transition metal). Later on, the electrochemical extraction of Na^+ from $Na_3V_2(PO_4)_3$ to $NaV_2(PO_4)_3$ was shown to occur following a two-phase reaction at 3.37 V versus Na^+/Na (Fig. 1) [10] the latter phase being isotypical with $NaTi_2(PO_4)_3$ [11-13]. Moreover, as shown by Yamaki *et al.* [8] and Patoux *et al.* [10], V^{3+} may be reduced to V^{2+} through the electrochemical or chemical insertion of one sodium per formula unit, towards $Na_4V_2(PO_4)_3$ at 1.65 V vs. Na^+/Na (for a theoretical capacity of 58.8 mA.h/g). These particular features offer the possibility of building symmetrical NVP / electrolyte / NVP batteries operating at 1.8 V, as recently demonstrated [14-16]. Up to now, to the best of our knowledge, no demonstration of reversible electrochemical extraction of Na^+ towards $V_2(PO_4)_3$ was demonstrated, similar to what was reported for the Li^+ counterpart NASICON B-$Li_3V_2(PO_4)_3$ [17, 18].

Importantly, these observations tend to indicate a strong discrepancy between the original result of Gopalakrishnan and the experimental electrochemical oxidation of V^{3+} to V^{4+} through the extraction of only two Na^+ out of three. As shown by Song et al. [19], galvanostatic extraction of Na+ from pure $Na_3V_2(PO_4)_3$ up to 4.5 V vs. Na does not permit of extracting more than two Na^+. Therefore, part of the "heavy" vanadium in the structural formula $Na_3V_2(PO_4)_3$ appears to be

useless and we undertook chemical substitutions within the NASICON framework so as to better understand the reasons for such limitation. In other words, we wanted to precisely determine if the final composition $NaV_2(PO_4)_3$ reached was due either to the impossibility of oxidizing V^{4+} to V^{5+} within the NASICON framework or to the impossibility of yielding a composition with less than one Na^+ in the framework. For this purpose, we investigated the possible substitution of part of vanadium by aluminum according to the structural formula $Na_3Al_yV_{2-y}(PO_4)_3$ ($0 \leq y \leq 0.5$). Such M/Al substitution has been shown previously to be possible into lithium- and sodium-based NASICON phases as an efficient method for improving the ionic conductivity [20]. The substitution of vanadium by aluminum has already been reported for the anti-NASICON composition A-$Li_3Al_yV_{2-y}(PO_4)_3$ (up to y = 0.5) [21-23] and for the NASICON B-$Li_3Al_yV_{2-y}(PO_4)_3$ obtained by ion exchange with the sodium analog B-$Na_3Al_yV_{2-y}(PO_4)_3$ (with y = 0.1) [24]. Up to now, no electrochemical investigation of these systems as positive electrodes in Na batteries has been reported. We report here on the synthesis, on the crystal structure and on the electrochemical activity of $Na_3Al_yV_{2-y}(PO_4)_3$ compositions : y = 0, 0.1, 0.25 and 0.5.

Experimental:

NASICON $Na_3Al_yV_{2-y}(PO_4)_3$ powders were prepared by solid state reaction in stoichiometric proportions from NH_4VO_3, NaH_2PO_4 and $Al[OC(CH_3)_3]_3$ precursors for y = 0, 0.1, 0.25, 0.5. NH_4VO_3 (Sigma-Aldrich 99%) and NaH_2PO_4 (Sigma-Aldrich 99%) were mixed and dissolved in hot water before aluminum tert-butoxide $Al[OC(CH_3)_3]_3$ (Sigma-Aldrich 99%), previously dissolved in absolute ethanol, was added dropwise. After slow evaporation of solvents, the remaining solid was successively grinded and gently heated up to 300°C as a pre-treatment to avoid uncontrolled volumetric expansion of the powder. After grinding the powder, a two steps heat treatment was performed in a tubular furnace under argon-hydrogen (90:10 vol.%) atmosphere at 400°C for 5 hours and at 750°C for 12 hours in order to reduce V^{5+} into V^{3+}.

X-ray powder diffraction (XRD) diagrams were collected at 223K and 243K for $Na_3Al_yV_{2-y}(PO_4)_3$ compositions and $Na_3V_2(PO_4)_3$ respectively. The samples were placed under primary vacuum within an Anton Paar TTK450 chamber mounted in a Bruker D8 diffractometer

using the Cu-$K_{\alpha1}/K_{\alpha2}$ radiations and mounted in θ-θ configuration. High quality diffraction patterns were recorded overnight between 2θ = 10° and 2θ = 100° by steps of 4.5 s/0.01°. Part of the same samples were also sealed inside 0.5 mm diameter glass capillaries under argon atmosphere, and sent to the 11-BM at the APS Argonne, USA, for high resolution synchrotron X-ray diffraction data acquisition at 473 K. To this end, a constant wavelength of 0.413355 Å was used in the range 1-50°, with a step size of 0.001°.

Operando X-ray diffraction patterns, recorded during electrochemical cycling, were obtained from a Bruker D8 diffractometer using the Cu-$K_{\alpha1}/K_{\alpha2}$ radiations, mounted in θ-θ configuration between 2θ = 10° and 2θ = 45° for various acquisition times depending on the current rate and using the Be-containing electrochemical cell described in [25]. Data treatment and sequential Rietveld refinements were performed using the FullProf Suite [26].

Differential Scanning Calorimetry (DSC) measurements were performed using a Mettler Toledo DSC1 apparatus operating at heating/cooling rates of 10 K/min between -30 and 250°C under argon atmosphere.

Electrochemical tests were performed on a 83:17 wt% mixture of the active material and Super P carbon, obtained by ball-milling in a SPEX 8000 mixer (2 stainless steel balls of 2g, 15min). In Swagelok®-type cells, about 10-15 mg of the electrochemically active mixture were used as the positive electrode, separated from a sodium disk by two sheets of Whatman® GF/D borosilicate glass fiber soaked in a 1 M molar solution of NaPF6 in EC/DMC 1:1. Galvanostatic tests were conducted with a Biologic® VMP potentiostat controlled by means of the EC-Lab® software. For *operando* XRD measurements, 25-30 mg of the active mixture were loaded in our *in situ* cell behind an Al-protected Be window [25]. Galvanostatic tests were conducted with an Apple® Mac Pile potentiostat.

Results and Discussion

a - Structural considerations

The most common space group encountered for describing the crystal structure of NASICON compositions is rhombohedral, *R*-3*c*. In certain conditions, low temperature and/or specific composition ranges for instance, the lattice may be distorted to a lower symmetry (monoclinic in most cases) due to Na^+ ordering on both M(1) and M(2) crystallographic sites, as extensively documented in the literature of the mid 70's - early 80's [11, 27, 28]. This is the case, as well, for $Na_3V_2(PO_4)_3$ (NVP) [10, 15, 17], $Na_3Ti_2(PO_4)_3$ [11, 29], and $Na_3Al_2(PO_4)_3$ [30]. Contrary to what is reported in many recent publications (which refer to a rhombohedral indexation of the diffraction patterns), we wish to stress that $Na_3V_2(PO_4)_3$ indeed crystallizes in a distorted monoclinic unit-cell at room temperature with complex phenomena of Na^+ ion ordering [15, 17]. This leads to a set of superstructure diffraction peaks, indicated in figure 2, that disappear upon heating at moderate temperature (~200°C) in full accordance with reversible thermal effects observed by DSC [15, 31]. Order-disorder transitions within the Na^+ sub-lattice are typical of Natrium Super Ionic CONductors (NASICON) and are associated with a randomization of the Na^+ positions and a lowering of the activation energy for ionic conduction.

The overnight XRD data collected at low temperature (from -30°C to -50°C) are reported in Figure 2 for y = 0, 0.1, 0.25 and 0.5 in $Na_3Al_yV_{2-y}(PO_4)_3$ together with the synchrotron pattern of $Na_3Al_{0.5}V_{1.5}(PO_4)_3$ at 200°C. As a first observation, we show here that the $Na_3Al_yV_{2-y}(PO_4)_3$ solid solution can be extended up to ~ 0.5 with a progressive shift of most of the diffraction peaks towards higher 2θ angles, as a result of progressive unit-cell contraction when Al substitutes for V in $Na_3Al_yV_{2-y}(PO_4)_3$ (Table 1). As demonstrated by temperature-controlled experiments the series of "new" small-intensity diffraction peaks encountered for the low temperature forms of $Na_3Al_yV_{2-y}(PO_4)_3$ are not related with impurities within our powders but characteristic of their crystal structure as they disappear upon heating (and come back under subsequent cooling). As a result, the XRD pattern of $Na_3Al_{0.5}V_{1.5}(PO_4)_3$ recorded at 200°C can be fully indexed in the *R*-3*c* space group (Table 1).

These structural considerations obtained through X-ray diffraction data can be nicely correlated with the DSC data recorded for the three compositions y = 0.1, 0.25, 0.5 in $Na_3Al_yV_{2-y}(PO_4)_3$, plotted in figure 3 together with high resolution XRD data. Below room temperature, all the

compositions show pronounced monoclinic distortions (indexed in space group *C*2 [31]) while they can all be fully indexed in the rhombohedral space group *R*-3*c* at 200°C (Table 1). Upon increasing the Al content, the temperature at which the *R*-3*c* is stabilized is lowered, from 180°C for $Na_3V_2(PO_4)_3$ [15] down to ~145°C for $Na_3V_{1.75}Al_{0.25}(PO_4)_3$. Noticeably, the crystallinity of our powders seems to decrease with Al content increasing, as witnessed by a continuous increase of the FWHM of the diffraction peaks, from $Na_3V_2(PO_4)_3$ to $Na_3V_{1.5}Al_{0.5}(PO_4)_3$. This may be the reason why the order-disorder transition upon heating $Na_3V_{1.5}Al_{0.5}(PO_4)_3$ is hardly detectable by DSC.

b – Electrochemical insertion of Na^+ into $Na_3Al_yV_{2-y}(PO_4)_3$

As already mentioned in the recent literature, the electrochemical insertion of Na^+ into $Na_3V^{III}_2(PO_4)_3$ leads to $Na_4V^{III}V^{II}(PO_4)_3$ through a biphasic mechanism at 1.65 V vs. Na^+/Na for a limited theoretical gravimetric capacity of 58.8 mA.h/g (figure 1). The reason for such a low capacity is nested in the limited interstitial space available for Na^+ in the NASICON framework, equal to a maximum of 4 Na^+ per $M_2(XO_4)_3$ structural formula [12, 13, 28, 32]. In other words, only half of vanadium is utilized upon electrochemical reduction and its partial substitution would not, then, induce a penalty in terms of theoretical capacity. As displayed on the right part of figure 4, one sodium ion per structural formula was successfully inserted (at a regime of C/20) in each of the $Na_3Al_yV_{2-y}(PO_4)_3$ compositions, upon two sets of poorly separated (~50 mV) dx/dV derivative peaks in approximate ratios of 1/10 (figure S1). The experimental gravimetric capacities obtained slightly increase with the Al content but the most prominent feature is that the energy of the V^{3+}/V^{2+} redox couple is progressively shifted to higher values, i.e. lower operating voltage vs. Na^+/Na, when the Al content increases (1.6 V vs. Na^+/Na for $Na_3V_{1.5}Al_{0.5}(PO_4)_3$ and 1,65 V for $Na_3V_2(PO_4)_3$). This may be correlated with the observed decrease of the V-O bond lengths when V is substituted by Al (hence with stronger covalency and as a consequence higher position of the V^{3+}/V^{2+} redox couple).

One of the above mentioned compositions, $Na_3Al_{0.25}V_{1.75}(PO_4)_3$, was selected to perform an *operando* X-ray diffraction experiment during full discharge / charge of the battery. As displayed in figure 5, the insertion / extraction of 1 Na^+ into $Na_3Al_{0.25}V_{1.75}(PO_4)_3$ is fully reversible, through

a biphasic mechanism, mostly. Careful examination of the *operando* XRD data reveals a small solid solution domain, for the first region of Na^+ insertion, up to ~$Na_{3.1}Al_{0.25}V_{1.75}(PO_4)_3$ (see Fig. 5, scan 3). Subsequently, two phases coexist for the entire discharge, the proportions of which varying continuously up to the final single phase $Na_4Al_{0.25}V_{1.75}(PO_4)_3$ (Table 1). However, the peaks positions of each phase are moving slightly during the process so that at mid-(dis)charge, the pattern is not a linear combination of both end members. This kind of unusual behavior was also observed for other chemical systems such as Li_xVPO_4O [33] and $Li_yMn_2O_4$ [34]. Overall, the insertion of one Na^+ within $Na_3Al_{0.25}V_{1.75}(PO_4)_3$ yields a unit-cell expansion of $\Delta V/V = + 3\%$ with a sharp decrease of the c/a ratio, as commonly encountered in NASICON compositions upon filling the Na(2) crystallographic site.

c – Electrochemical extraction of Na^+ from $Na_3Al_yV_{2-y}(PO_4)_3$

The electrochemical extraction of two sodium ions from $Na_3V^{III}_2(PO_4)_3$ leads to $NaV^{IV}_2(PO_4)_3$ through a biphasic mechanism at 3.37 vs. Na^+/Na for an overall theoretical gravimetric capacity of 117.6 mAh/g. As mentioned in the introduction part of this paper, vanadium is oxidized from V^{3+} to V^{4+} in $NaV^{IV}_2(PO_4)_3$ (Table 2) and the presence of one remaining Na^+ in the framework opens the door, theoretically, for the possible oxidation of V^{4+} to V^{5+} towards the final composition $V^{V}V^{IV}(PO_4)_3$. Apart from the report of Gopalakrishnan [9], this phase has never been reported so far although V^{5+} - containing phosphates have been mentioned previously, such as for $Li_3V_2(PO_4)_3$ [10, 17, 18, 35] and $LiVOPO_4$ [33, 36] positive electrodes in Li batteries. At this point, it is hence reasonable to argue that the capacity limitation in $Na_3V_2(PO_4)_3$ comes from a price to pay too high in energy for extracting the remaining Na^+ from the Na(1) site as the oxidation of V^{3+} to V^{4+} and then to V^{5+} was previously observed in other structural units.

Consequently, mixed $Na_3Al_yV_{2-y}(PO_4)_3$ compositions are interesting to investigate as they may render the V^{4+}/V^{5+} redox couple accessible. The reversible electrochemical oxidation (extraction of Na^+) of each $Na_3Al_yV_{2-y}(PO_4)_3$ composition (y = 0.1, 0.25, 0.5) within the 2.4 – 3.8 V voltage window is displayed on the left part of figure 4. Under these conditions, only the V^{3+}/V^{4+} redox couple is active so that the charge capacity decreases progressively when the overall content of vanadium decreases (from 117.6 mAh/g for $Na_3V_2(PO_4)_3$ down to 90.6 mAh/g for

$Na_3Al_{0.5}V_{1.5}(PO_4)_3$). Importantly, contrary to $Na_3V_2(PO_4)_3$, the extraction of Na^+ from $Na_3Al_{0.25}V_{1.75}(PO_4)_3$ and $Na_3Al_{0.5}V_{1.5}(PO_4)_3$ occurs through two distinct redox steps separated by ~0.04 V while the "average" V^{3+}/V^{4+} remains at a value of 3.37 V vs. Na^+/Na (Figure S1). These two redox steps are the signature of two biphasic reactions that occur upon charge / discharge for a given starting composition, as illustrated by the *operando* XRD experiment displayed in figure 6. The extraction of Na^+ from $Na_3Al_{0.25}V_{1.75}(PO_4)_3$ towards $Na_{1.25}Al_{0.25}V_{1.75}(PO_4)_3$ (Table 2) generates an intermediate single phase mixed valent (V^{3+} and V^{4+}) composition of ~ $Na_{2.1}Al_{0.25}V_{1.75}(PO_4)_3$ whose lattice parameters vary slightly upon the two-phase domains as already witnessed in other systems [33, 34]. The overall charge / discharge electrochemical reaction is, structurally speaking, highly reversible as the XRD pattern of the pristine phase is fully recovered after one cycle.

If the cutoff voltage upon charge is set to an upper value of 4.2 V vs. Na^+/Na, additional electrochemical activity is encountered at ~3.95 V vs. Na^+/Na, for the V^{4+} / V^{5+} redox couple. As shown in figure 7, the extraction of Na^+ from $Na_3Al_{0.5}V_{1.5}(PO_4)_3$ first occurs at ~3.37 V through the oxidation of 1.5 vanadium from V^{3+} to V^{4+}, i.e. towards the composition $Na_{1.5}Al^{III}_{0.5}V^{IV}_{1.5}(PO_4)_3$, then followed by the additional extraction of Na^+ towards $Na_{1.0}Al^{III}_{0.5}V^{IV}_{1.0}V^{V}_{0.5}(PO_4)_3$ upon oxidation of 0.5 vanadium from V^{4+} to V^{5+}. Hence, concomitant with the slight increase in gravimetric capacity upon substitution of part of the inactive vanadium by aluminum in $Na_3Al_yV_{2-y}(PO_4)_3$, the Al substitution increases significantly the energy density of NVP-type NASICON electrodes, from 396.3 Wh/kg for $Na_3V_2(PO_4)_3$ to 424.6 Wh/kg for $Na_3Al_{0.5}V_{1.5}(PO_4)_3$. The corresponding *operando* XRD experiment up to 4.2 V vs. Na^+/Na, is displayed in figure 8. As for $Na_3Al_{0.25}V_{1.75}(PO_4)_3$, two distinct bi-phasic regions at 3.34 V and 3.39 V vs. Na^+/Na are first encountered at an average voltage of ~3.37 V vs. Na^+/Na for the oxidation of V^{3+} into V^{4+}. The *operando* experiment reveals, additionally, that the $V^{4+} \rightarrow V^{5+}$ electrochemical reaction occurs through a single phase mechanism centered at ~3.95 V vs. Na^+/Na. From $Na_{1.5}Al^{III}_{0.5}V^{IV}_{1.5}(PO_4)_3$ to $Na_{1.0}Al^{III}_{0.5}V^{IV}_{1.0}V^{V}_{0.5}(PO_4)_3$ at the end of oxidation, the lattice parameters vary continuously, as determined in the space group *R*-3*c*, to reach an overall V/Z value of 218.4 $Å^3$.

Conclusions

This study, focused on the crystal chemistry of new compositions of general formula $Na_{3-x}Al_yV_{2-y}(PO_4)_3$ has shown, for the first time, that the extend of V / Al substitution in this NASICON framework, can be as high as y = ~ 0.5, which modifies significantly the electrochemical properties of this important family of materials as positive electrode for Na batteries. Compared with the $Na_3V_2(PO_4)_3$ composition, both the theoretical gravimetric capacity (due to substitution of V by lighter Al) and the average operating voltage (due to the access to the V^{4+}/V^{5+} redox couple) are higher. So far, we did not succeed to determine if the practical energy and power densities of these electrodes are indeed improved significantly compared with pure $Na_3V_2(PO_4)_3$. Future studies will focus on the evaluation of the rate capabilities and cycle efficiencies of this important class of new compositions.

Despite our repeated synthesis attempts, the hypothetical composition $Na_3AlV(PO_4)_3$ could not be obtained, for which we envisage a theoretical capacity of 120.8 mAh/g operating for 50 % of this capacity at 3.37 V vs. Na (V^{3+} / V^{4+}) and for the remaining 50% at 3.95 V vs. Na (V^{4+}/V^{5+}) for an overall expected energy density of 458.4 Wh/kg ($Na_3\ V^{3+}{}_1\ Al_1\ (PO_4)_3 \rightarrow Na_1\ V^{5+}{}_1\ Al^{3+}{}_1\ (PO_4)_3$)

Acknowledgments

The Ministry of Higher Education & Research of France is gratefully acknowledged for the financial support of F.L. via a “Contrat Doctoral” of UPJV Amiens. Use of the Advanced Photon Source (APS) beam line 11-BM at Argonne National Laboratory, under fast access proposal n° 42779, was supported by the U. S. Departement of Energy, Office of Science, Office of Basic Energy Sciences, under Contract no. DE-AC02-06CH11357.

References:

[1] K. Saravanan, C.W. Mason, A. Rudola, K.H. Wong, P. Balaya, *Adv. Ener. Mater.*, 2013, **3**, 444-450.
[2] S. Li, Y. Dong, L. Xu, X. Xu, L. He, L. Mai, *Adv. Mater.*, 2014, **26**, 3545-3553.
[3] P. Nie, Y. Zhu, L. Shen, G. Pang, G. Xu, S. Dong, H. Dou, X. Zhang, *J. Mater. Chem. A*, 2014, **2,** 18606-18612.
[4] L. Si, Z. Yuan, L. Hu, Y. Zhu, Y. Qian, *J. Power Sources*, 2014, **272,** 880-885.
[5] C. Zhu, K. Song, P.A. van Aken, J. Maier, Y. Yu, *Nano Letters*, 2014, **14**, 2175-2180.
[6] Q. An, F. Xiong, Q. Wei, J. Sheng, L. He, D. Ma, Y. Yao, L. Mai, *Adv. Ener. Mater.*, 2015, DOI: 10.1002/aenm.201401963).
[7] H. Li, Y. Bai, F. Wu, Y. Li, C. Wu, *J. Power Sources*, 2015, **273,** 784-792.
[8] Y. Uebou, T. Kiyabu, S. Okada, J.-i. Yamaki, *The Reports of Institute of Advanced Material Study*, 16 (2002).
[9] J. Gopalakrishnan, K.K. Rangan, *Chem. Mater.*, 1992, **4**, 745-747.
[10] S. Patoux, PhD in Materials Science, Université de Picardie Jules Verne, Amiens, France, (2003) p.212.
[11] C. Delmas, A. Nadiri, J.L. Soubeyroux, *Solid State Ionics*, 1988, **28-30,** 419-423.
[12] C. Masquelier, L. Croguennec, *Chem. Rev.,* 2013, **113(8)***,* 6552-6591
[13] S. Patoux, G. Rousse, J.-B. Leriche, C. Masquelier, *Chem. Mater.*, 2003, **15,** 2084-2093.
[14] Y. Noguchi, E. Kobayashi, L.S. Plashnitsa, S. Okada, J.-i. Yamaki, *Electrochimica Acta*, 101 (2013) 59-65.
[15] F. Lalère, J.B. Leriche, M. Courty, S. Boulineau, V. Viallet, C. Masquelier, V. Seznec, *J. Power Sources*, 2014, **247**, 975-980.
[16] L.S. Plashnitsa, E. Kobayashi, Y. Noguchi, S. Okada, J.-i. Yamaki, *J. Electrochem. Soc.*, 2010, **157,** 536-543.
[17] J. Gaubicher, C. Wurm, G. Goward, C. Masquelier, L. Nazar, *Chem. Mater.*, 2000, **12**, 3240-3242.
[18] S. Patoux, C. Wurm, M. Morcrette, G. Rousse, C. Masquelier, *J. Power Sources*, 2003, **119-121,** 278-284.
[19] W. Song, X. Ji, Z. Wu, Y. Zhu, Y. Yang, J. Chen, M. Jing, F. Li, C. E. Banks, *J. Mater. Chem. A*, 2014, **2**, 5358-5362.
[20] F.E. Mouahid, M. Zahir, P. Maldonado-Manso, S. Bruque, E.R. Losilla, M.A.G. Aranda, A. Rivera, C. Leon, J. Santamaria, *J. Mater. Chem.*, 2001, **11**, 3258-3263.
[21] J. Barker, R.K.B. Gover, P. Burns, A. Bryan, *J. Electrochem. Soc.*, 2007, 154, 307-313.
[22] D. Ai, K. Liu, Z. Lu, M. Zou, D. Zeng, J. Ma, *Electrochimica Acta*, 2011, **56, 2**823-2827.
[23] A.R. Cho, J.N. Son, V. Aravindan, H. Kim, K.S. Kang, W.S. Yoon, W.S. Kim, Y.S. Lee, *J. Mater. Chem.*, 2012, **22** 6556-6560.
[24] Y. Lu, L. Wang, J. Song, D. Zhang, M. Xu, J.B. Goodenough, *J. Mater. Chem. A*, 2013, **1,** 68-72.
[25] J.B. Leriche, S. Hamelet, J. Shu, M. Morcrette, C. Masquelier, G. Ouvrard, M. Zerrouki, P. Soudan, S. Belin, E. Elkaïm, F. Baudelet, *J. Electrochem. Soc.*, 2010, **157,** 606-610.
[26] J. Rodriguez-Carvajal, *Phycica B*, 1993, 55-59.
[27] F. d'Yvoire, M. Pintard-Scrépel, E. Bretey, M. de la Rochère, *Solid State Ionics*, 1983, **9–10**, 851-857.
[28] J.B. Goodenough, H.Y.P. Hong, J.A. Kafalas, *Mat. Res. Bull.*, 1976, **11,** 203-220.
[29] H. Kabbour, D. Coillot, M. Colmont, C. Masquelier, O. Mentré, *J. Amer. Chem. Soc.*, 2011, **133**, 11900-11903.
[30] F. Brunet, N. Bagdassarovb, R. Miletich, *Solid State Ionics*, 2003, **159**, 35-47.
[31] J.-N. Chotard, R. David, G. Rousse, O. Mentré, C. Masquelier, *Chem. Mater.*, submitted.
[32] F. Hatert, *Acta Cryst. E*, 2009, **65**, 30.

[33] M. Bianchini, J.M. Ateba-Mba, P. Dagault, E. Bogdan, D. Carlier, E. Suard, C. Masquelier, L. Croguennec, *J. Mater. Chem. A*, 2014, **2,** 10182-10192.
[34] M. Bianchini, E. Suard, L. Croguennec, C. Masquelier, *J. Phys. Chem. C*, 2014, **118,** 25947-25955.
[35] D. Morgan, G. Ceder, M.Y. Saïdi, J. Barker, J. Swoyer, H. Huang, G. Adamson, *Chem. Mater.*, 2002, **14**, 4684-4693.
[36] J. Gaubicher, T. Le Mercier, Y. Chabre, J. Angenault, M. Quartona, *J. Electrochem. Soc.*, 1999, **146**, 4375-4379.

Tables :

Table 1: Lattice parameters at -50°C (left) and at 200°C (right) of $Na_3Al_yV_{2-y}(PO_4)_3$ pristine compositions, determined by full pattern matching of XRD data.

	223 K (-50°C) : *C*2					**473 K (200°C) : *R*-3*c***			
y	***a* (Å)**	***b* (Å)**	***c* (Å)**	***β* (°)**	***V/Z* (Å^3)**	***a* (Å)**	***c* (Å)**	***c/a***	***V/Z* (Å^3)**
0.1	15.134(3)	8.724(2)	21.624(6)	90.22(1)	237.94	8.7235(6)	21.888(3)	2.509	240.42
0.25	15.10(1)	8.709(6)	21.61(1)	90.25(1)	236.83	8.7014(3)	21.866(2)	2.513	238.96
0.5	15.00(1)	8.66(1)	21.53(2)	90.29(1)	233.10	8.666(2)	21.769(6)	2.512	235.97

Table 2: Lattice parameters of $Na_xAl_yV_{2-y}(PO_4)_3$ compositions obtained upon Na^+ insertion or extraction (indexed in equivalent *R*-3*c* for comparison purpose)

		a (Å)	*c* (Å)	*c/a*	*V/Z* (Å^3)
V^{3+}/V^{2+}	$Na_4V_2(PO_4)_3$	8.94(1)	21.36(2)	2.39	246.3
	$Na_4Al_{0.25}V_{1.75}(PO_4)_3$	8.90(1)	21.35(1)	2.40	244.4
	$Na_4Al_{0.5}V_{1.5}(PO_4)_3$	8.86(3)	21.36(2)	2.41	242.3
V^{3+}	$Na_3V_2(PO_4)_3$	8.72(2)	21.78(6)	2.50	239.0
	$Na_3Al_{0.25}V_{1.75}(PO_4)_3$	8.70(1)	21.66(3)	2.49	236.7
	$Na_3Al_{0.5}V_{1.5}(PO_4)_3$	8.66(1)	21.67(3)	2.50	234.6
V^{4+}/V^{3+}	$Na_{2.125}Al_{0.25}V_{1.75}(PO_4)_3$	8.56(1)	21.56(3)	2.52	228.3
	$Na_{2.25}Al_{0.5}V_{1.5}(PO_4)_3$	8.55(1)	21.53(3)	2.52	227.2
V^{4+}	$Na_{1.0}V_2(PO_4)_3$	8.42(1)	21.47(3)	2.55	219.6
	$Na_{1.25}Al_{0.25}V_{1.75}(PO_4)_3$	8.44(1)	21.47(3)	2.54	220.6
	$Na_{1.5}Al_{0.5}V_{1.5}(PO_4)_3$	8.45(1)	21.46(3)	2.54	221.2
V^{5+}/V^{4+}	$Na_{1.0}Al_{0.5}V_{1.5}(PO_4)_3$	8.39(1)	21.50(3)	2.56	218.4

Figures:

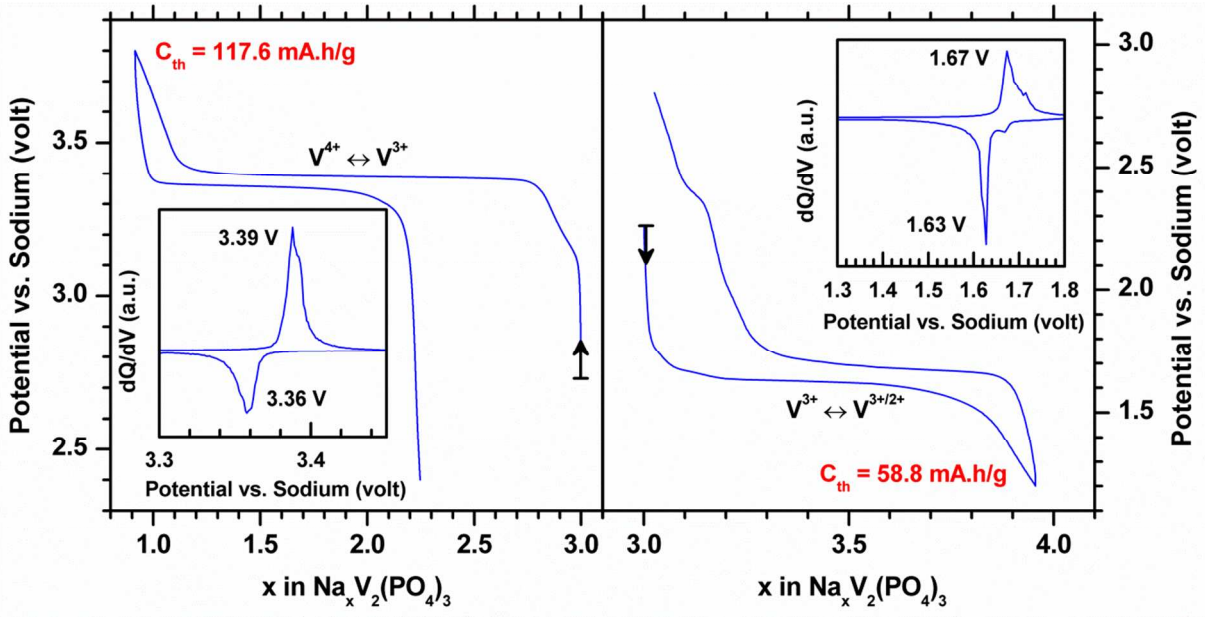

Fig. 1: Electrochemical signatures of $Na_3V_2(PO_4)_3$ electrodes upon Na^+ extraction (left) or Na^+ insertion (right). Galvanostatic data were recorded for a current rate corresponding to $1Na^+/20h$.

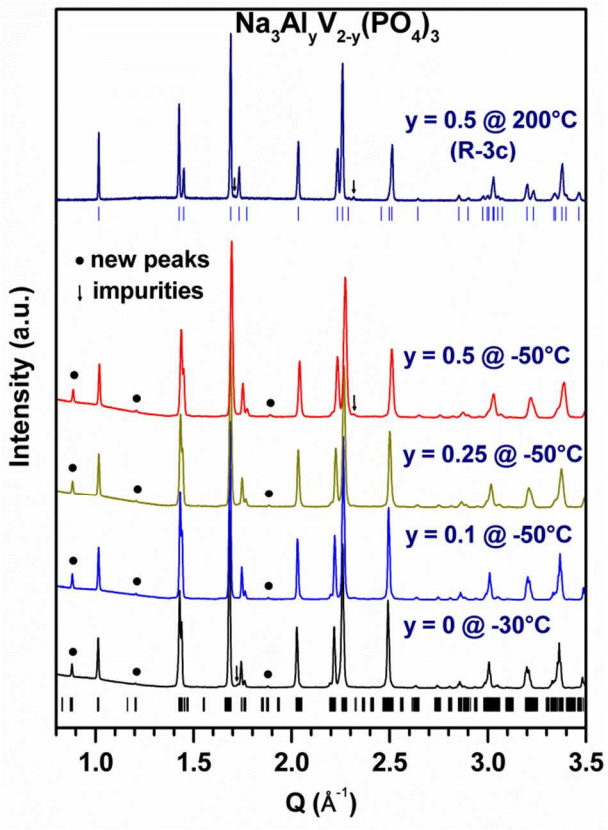

Fig. 2: X-ray diffraction patterns of $Na_3Al_yV_{2-y}(PO_4)_3$ compositions ($0 \leq y \leq 0.5$) recorded below room temperature and at 200°C for $Na_3Al_{0.5}V_{1.5}(PO_4)_3$ (top). The "new" diffraction peaks (•) refer to d_{hkl} values not indexable in the rhombohedral R-3c space group. Bragg positions corresponding to the monoclinic *C*2 cell are given. Minor "Impurities" refer to traces of V_2O_3 or to the incommensurate form of NVP (see [31]).

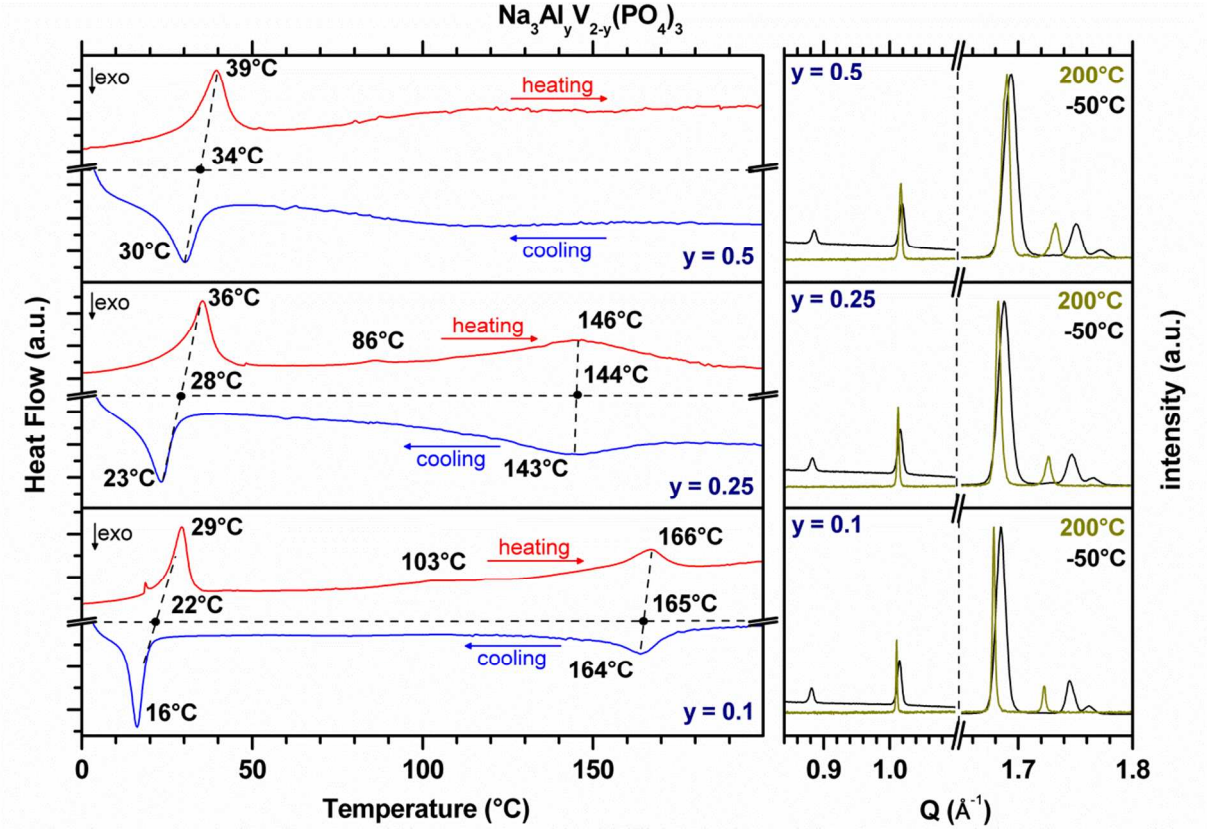

Fig. 3: (left) Differential scanning calorimetry data recorded under Ar at 10°/min for $Na_3Al_yV_{2-y}(PO_4)_3$ compositions. (right) selected regions of X-ray diffraction patterns for the corresponding low- (*C*2) and high-temperature (*R*-3*c*) phases recorded at APS (200°C) and in-house (-50°C).

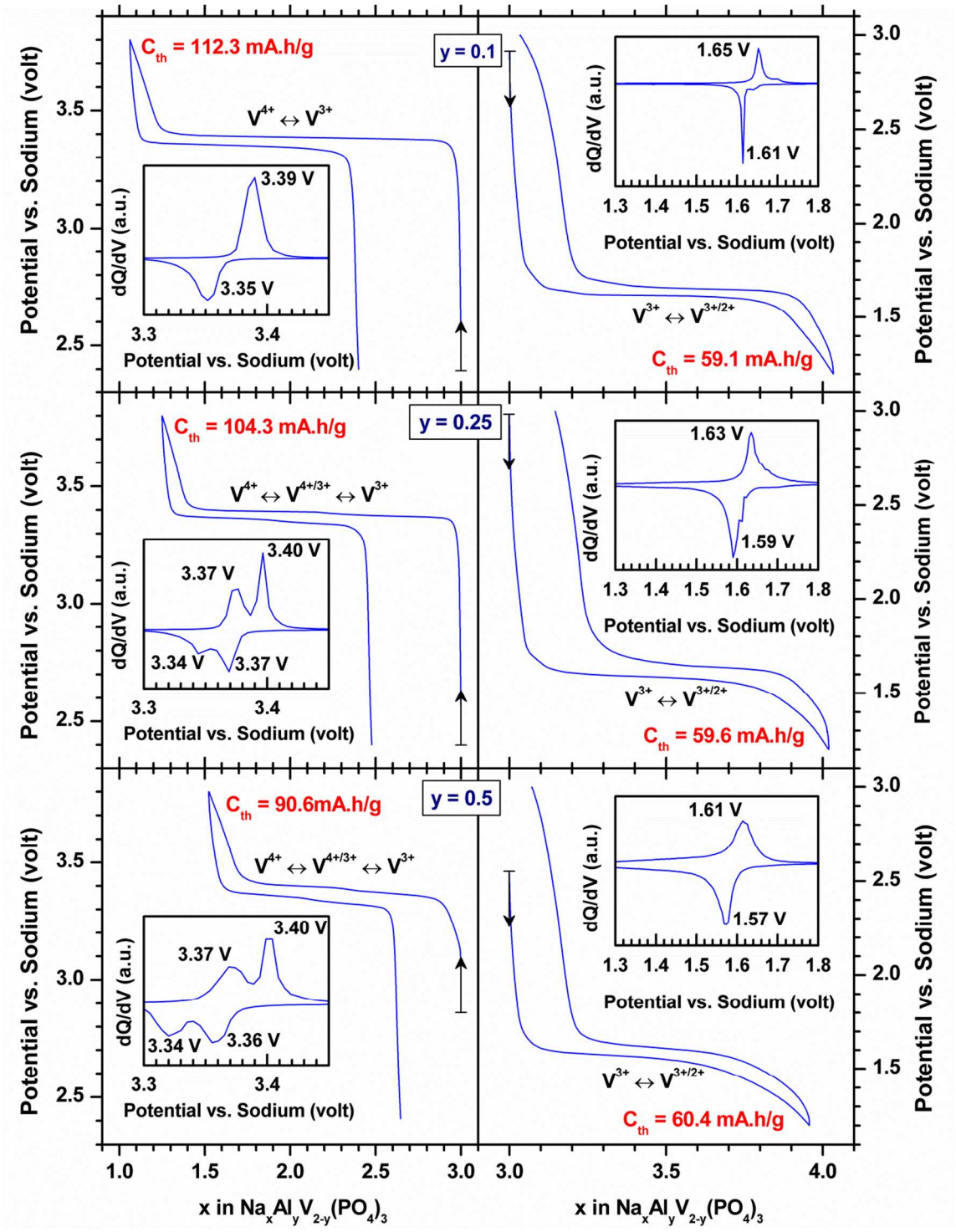

Fig. 4: Electrochemical signatures of $Na_3Al_yV_{2-y}(PO_4)_3$ electrodes upon Na^+ extraction (left) or Na^+ insertion (right). Galvanostatic data were recorded for a current rate corresponding to $1Na^+/20h$.

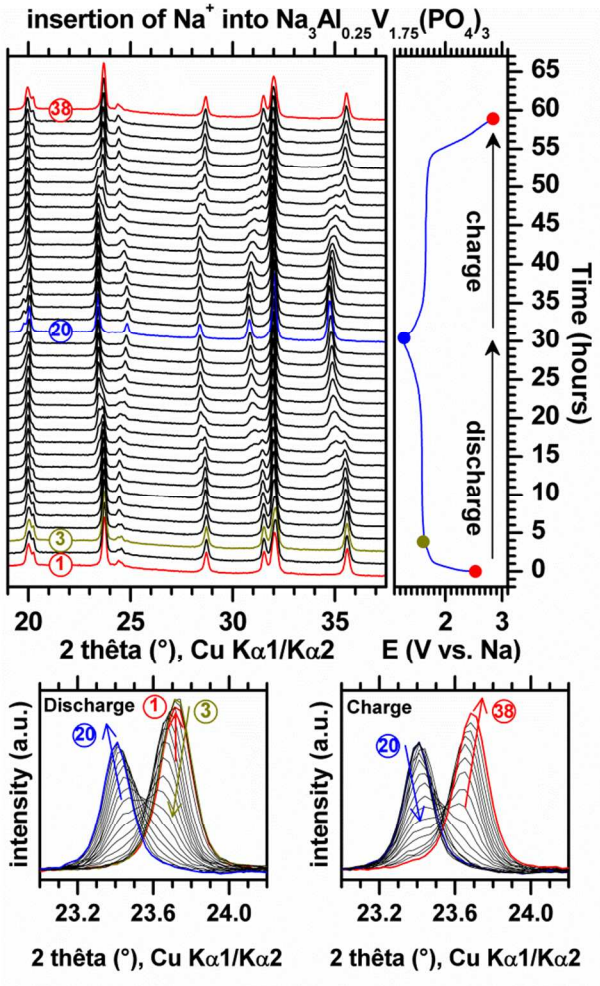

Fig. 5: (top) XRD patterns recorded *operando* for $Na_3Al_{0.25}V_{1.75}(PO_4)_3$ electrode upon galvanostatic discharge and charge (operating on the V^{3+}/V^{2+} couple) at a current rate corresponding to 1 Na^+/30h. (down) an enlarged view of the 23-24° region.

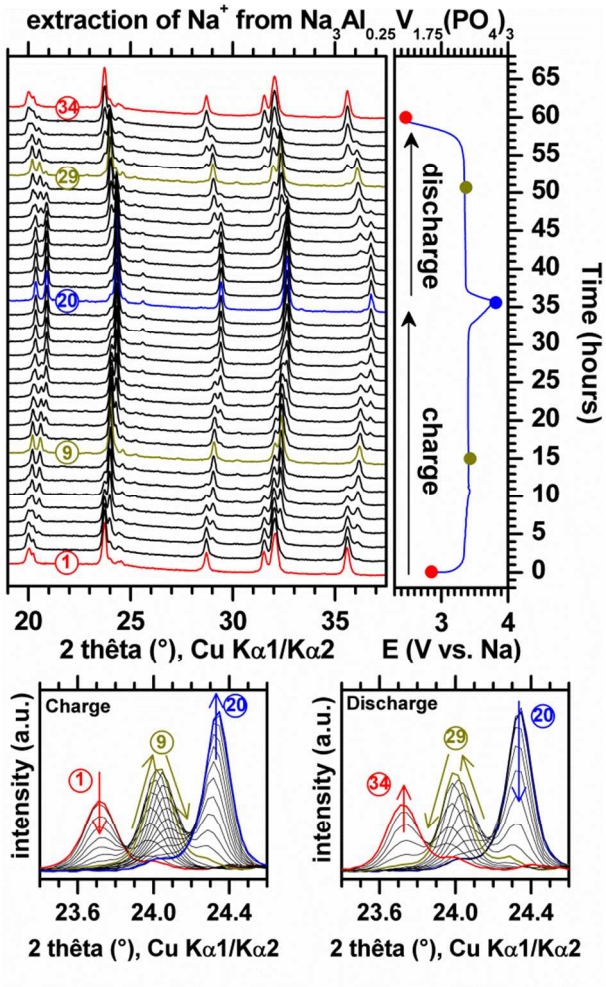

Fig. 6: (top) *operando* XRD patterns of Na//$NaPF_6$ 1M in EC:DMC (1:1)//$Na_3Al_{0.25}V_{1.75}(PO_4)_3$ cell upon galvanostatic charge and discharge at a current rate corresponding to 1 Na^+/20h up to 3.8 V and (down) an enlarged view of the 23.4-24.4° region.

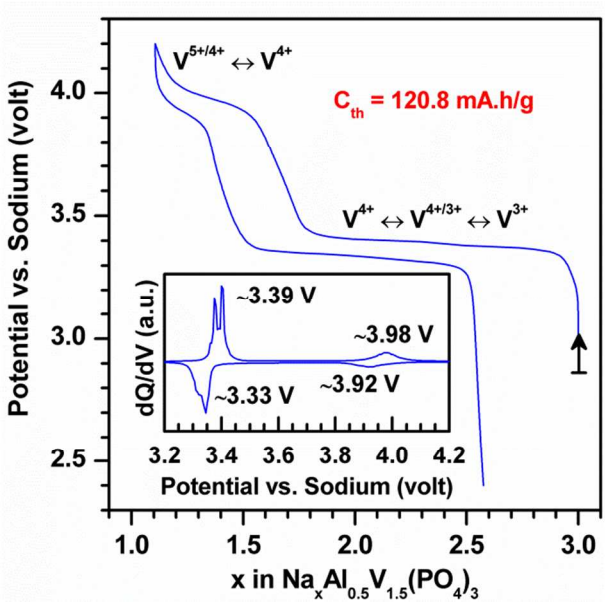

Fig. 7: Electrochemical signature of $Na_3Al_{0.5}V_{1.5}(PO_4)_3$ electrode upon Na^+ extraction/insertion. Galvanostatic data were recorded for a current rate corresponding to $1Na^+/20h$.

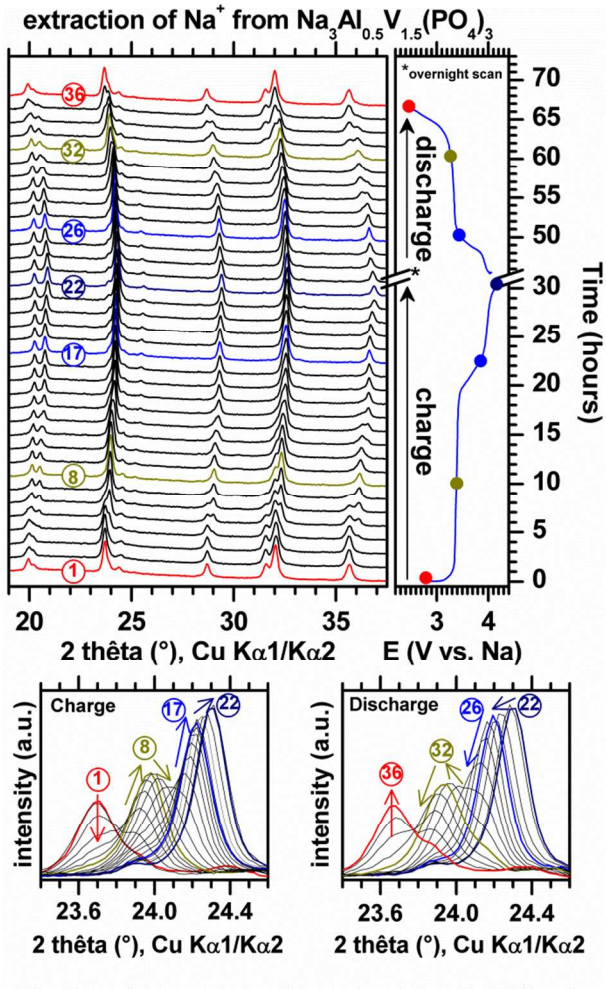

Fig. 8: (top) *operando* XRD patterns of Na//$NaPF_6$ 1M in EC:DMC (1:1)//$Na_3Al_{0.5}V_{1.5}(PO_4)_3$ cell upon galvanostatic charge at a current rate corresponding to 1 Na^+/15h up to 4.2 V and (down) an enlarged view of the 23.4-24.4° region.

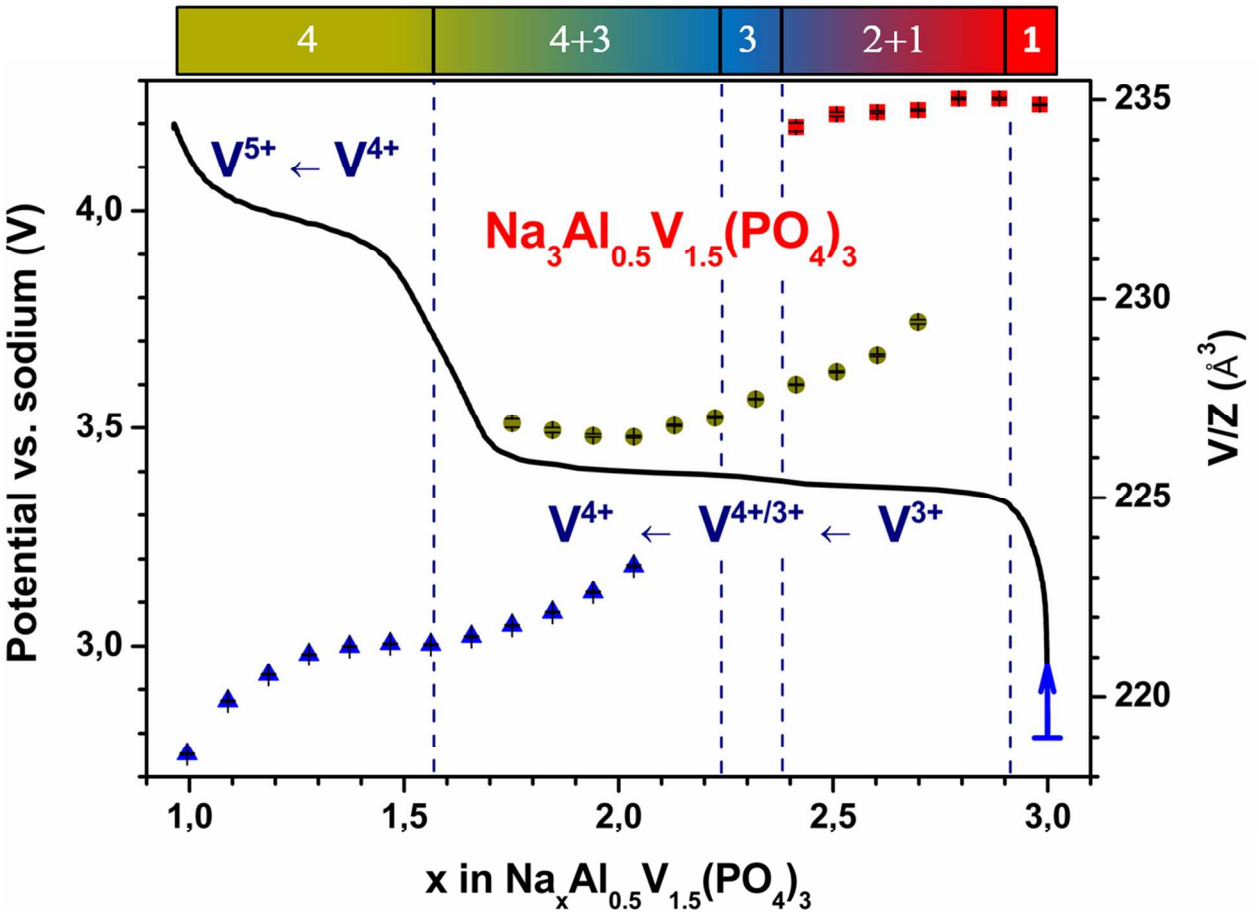

TOC

Supplementary figures:

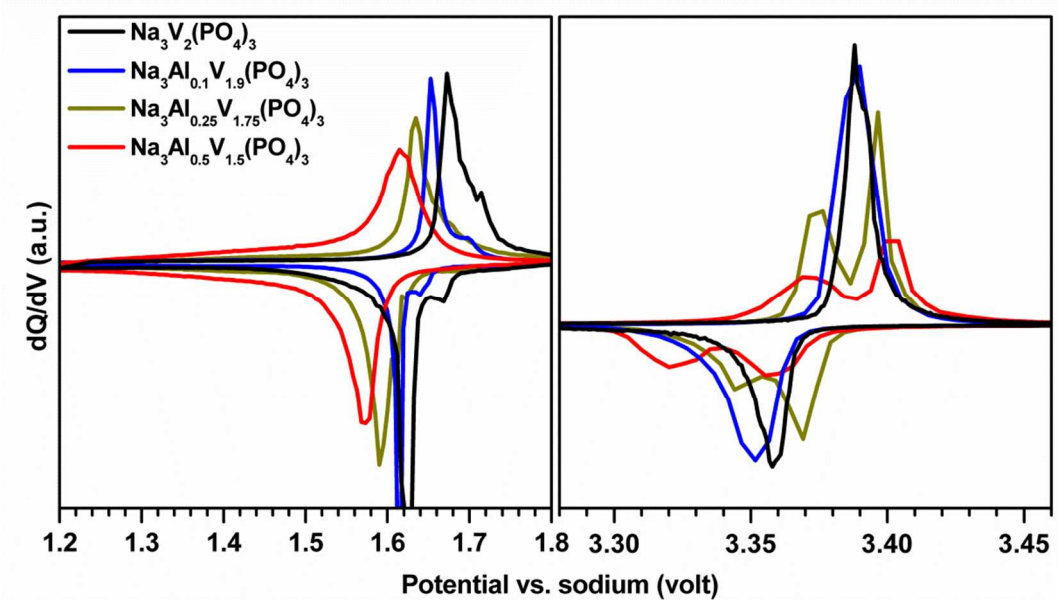

Fig. S1: Derivative electrochemical data upon Na^+ extraction/insertion from/into $Na_3Al_yV_{2-y}(PO_4)_3$ for y = 0, 0.1, 0.25, 0.5.

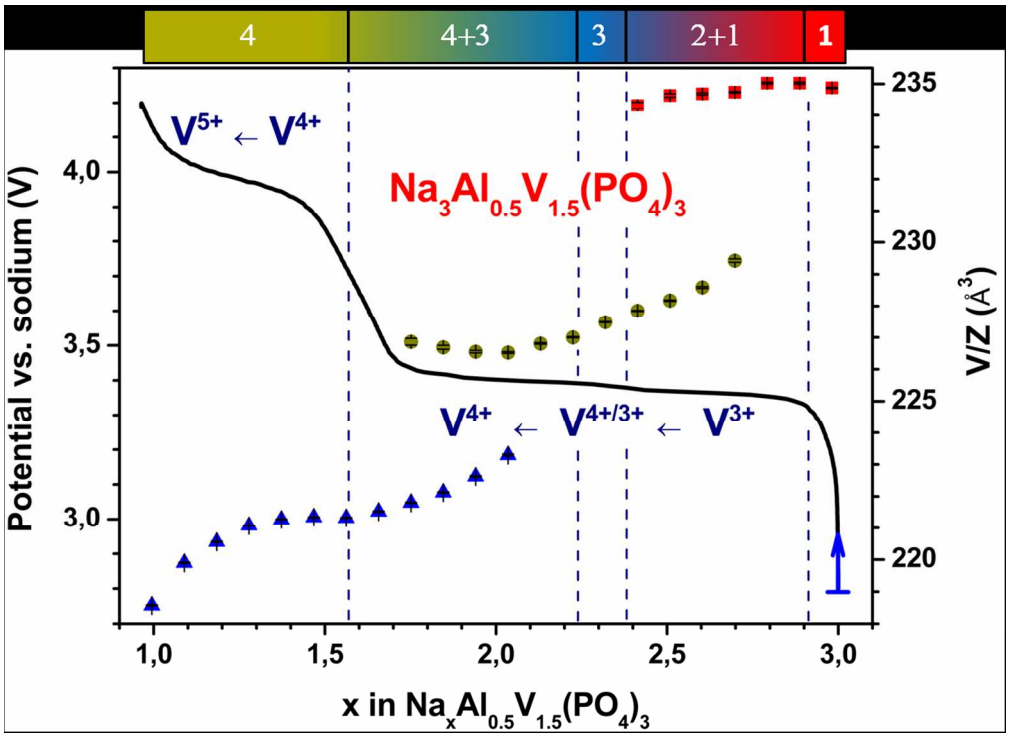

228x165mm (150 x 150 DPI)